Pramana – J. Phys. (2020) 94:54
https://doi.org/10.1007/s12043-019-1913-1

Analysis of ferrite nanoparticles in liquid

SOHAIL NADEEM[1,2], SHAFIQ AHMAD[3],* and NOOR MUHAMMAD[3]

[1]Mathematics and its Applications in Life Sciences; [2]Faculty of Mathematics and Statistics, Ton Duc Thang University, Ho Chi Minh City, Vietnam
[3]Department of Mathematics, Quaid i Azam University, Islamabad, Pakistan
*Corresponding author. E-mail: ashafiq@math.qau.edu.pk

MS received 25 July 2019; revised 17 November 2019; accepted 5 December 2019

Abstract. The foremost aim of the present paper is to explore the impact of heat transport phenomenon in a ferrofluid via magnetic dipole. Three distinct ferrite nanoparticles are discussed in the present study with water as the base fluid. Magnetic dipole existing in ferrite nanoparticles plays a significant role in controlling the momentum and thermal boundary layers. The partial differential equations (PDEs) are changed into nonlinear coupled ordinary differential equation (ODEs) by utilising similar transformations. Flow occurs due to linear stretching sheet. For the evaluation of heat flux, Fourier's law of heat conduction is employed. Effects of rising parameters on the magneto-thermomechanical coupling are examined numerically. The results indicate that the property of magneto-thermomechanical cooperation slows the motion of liquid particles, and accordingly, strengthen the heat transfer rate at the surface and skin friction coefficient. Further, Nusselt number enhances with larger solid volume fraction. A magnificent comparison with accessible results for definite cases has been made.

Keywords. Ferromagnetic nanofluid; water-based ferrite nanoparticles; heat transfer; magnetic dipole.

PACS No. 44.00

1. Introduction

A fluid which contains nanometre-sized particles is known as nanofluid. Nanofluids are designed colloidal interruption of nanoparticles in a base fluid. The nanoparticles used in nanofluids are usually made of carbon nanotubes, oxides, metals, or carbides. Base fluids are commonly ethylene glycol, water, and oil. In heat transfer, nanofluids have narrative properties that make them possibly helpful in numerous applications, counting chiller, boiler flue gas temperature reduction microelectronics, domestic refrigerator, heat exchanger, pharmaceutical processes, fuel cells, and engine cooling/vehicle thermal management. Base fluid shows low convective heat transfer and thermal conductivity compared to nanofluids [1,2]. Choi and Eastman [3] were the first to introduce the new class of nanofluids. Nadeem and Shahzadi [4] analysed theoretically the peristaltic flow embedded in nanoparticles over a curved channel. Sheikholeslami *et al* [5] studied the magnetohydrodynamic (MHD) CuO–water nanofluid inside a sinusoidal annulus with melting heat transfer. Tabassum *et al* [6] discussed the Cu–water micropolar nanofluid flow under the influence of microrotation and viscosity variation. Akbar *et al* [7] utilised the diverging (or non-uniform) tube to study the peristaltic nanofluid flow. Ramzan and Bilal [8] studied the elastico-viscous nanofluid in the presence of magnetic field and chemical reaction. Makinde [9] investigated the boundary layer flow of a nanofluid with viscous dissipation and Newtonian heating through a flat plate. Khamis *et al* [10] evaluated the water base nanofluid under the effect of variable viscosity and buoyancy force. Nadeem *et al* [11] demonstrated the feature of induced magnetic field in viscous Cu, Al_2O_3, and TiO_2 nanofluid flow through a static and moving wedge. Ma *et al* [12] explored the effect of magnetic field on forced convection and heat transfer of Ag–MgO nanofluid in an active heater and cooler channel. Sultan *et al* [13] declared the forced convective flow and heat-mass transfer features of cross nanofluid over a stretched bidirectional surface in the presence of activation energy and nonlinear thermal radiation. Recently, a few researchers discussed the features of mass and heat transfer in the presence of nanoparticles [14–16].

Ferrite nanoparticles (FNPs) have attracted considerable attraction because of their broad application in many fields, for example, in wastewater treatment, as

Published online: 12 March 2020

catalysts, in biomedical and electronic devices. Ferrites are generally non-conductive ferrimagnetic ceramic mixes obtained from iron oxides, for example, magnetite (Fe_3O_4) or hematite (Fe_2O_3) and oxides of different metals. In this paper, we discuss three distinct types of FNPs, such as nickel zinc ferrite ($NiZnFe_3O_4$), manganese zinc ferrite ($MnZnFe_3O_4$), and magnetic ferrite (Fe_3O_4), and water as the carrier fluid. Ferrite particles end up noticeably smaller than 128 nm [17] and they move toward becoming superparamagnetic which prohibit self-agglomeration as they display their magnetic behaviour just when an outer magnetic field is connected. Without magnetic field such fluids behave like normal nanofluid. The applications of ferromagnetic nanofluids studied by several scientists can be found in [18–21]. Sheikholeslami *et al* [22] examined Fe_3O_4–H_2O nanofluid over an elliptical wall. Zeeshan and Majeed [23] examined the Jeffery fluid flow in the presence of magnetic dipole. Vestal and Zhang [24] depicted the magnetic properties of $MnZnFe_3O_4$ under the influence of surface coordination. Andersson and Valnes [25] used the stretching sheet to describe the heated ferrofluid with magnetic dipole. Muhammad and Nadeem [26] numerically and analytically examined the drag fraction of different FNPs. Forced thermal transfer of multi-wall carbon nanotubes–iron oxide nanoparticles/water hybrid nanofluid within a partially heated-shaped channel was explored numerically by Ma *et al* [27]. The characteristics of viscous nanofluid flow are demonstrated in [28–32].

This article focusses on establishing the concept of FNPs such as $MnZnFe_3O_4$, $NiZnFe_3O_4$, and Fe_3O_4 theoretically, and water used as the base fluid. Ferrofluids are used in analytical instrumentation, and these fluids have numerous optical applications because of their refractive properties, that is, each grain, a micro-magnet, reflects light. These applications include measuring specific viscosity of a liquid placed between a polariser and an analyser, illuminated by a helium–neon laser [33,34]. The transformed equation is explained analytically and numerically by integrating the optimal homotopy analysis method (OHAM) and BVPh2-midpoint technique. The evaluation of different FNPs is completed in the study of velocity field, temperature distribution, heat transfer rate, and wall shear stress. The physical parameters are described through graphs and tables.

1.1 *Flow analysis*

Consider the laminar, incompressible, and two-dimensional viscous boundary layer flow of the ferromagnetic $MnZnFe_3O_4$–H_2O, $NiZnFe_3O_4$–H_2O, along with Fe_3O_4–H_2O nanofluids past a stretching surface. The impact of the magnetic dipole is considered so that its centre lies on the x-axis at a distance d from the x-axis. Due to stretching of the surface, the nanofluid flow is produced. The surface stretches with the wall velocity $U_w = S_1 x$, where S_1 is a constant and the temperature at the ambient fluid and stretching surface are $\tilde{T} = \tilde{T}_\infty$ and $\tilde{T} = \tilde{T}_w$. The direction of the magnetic field lines due to the magnetic dipole are in the positive x-direction. The physical representation for the flow is shown in figure 1. To make ferrofluid saturate, the magnetic dipole gives rise to magnetic field of significant strength. The temperature of the liquid away from the surface is measured at $\tilde{T} = \tilde{T}_\infty$ and $\tilde{T}_w < \tilde{T}_\infty < \tilde{T}_c$, where $\tilde{T}_c$, the Curie temperature, is more prominent than

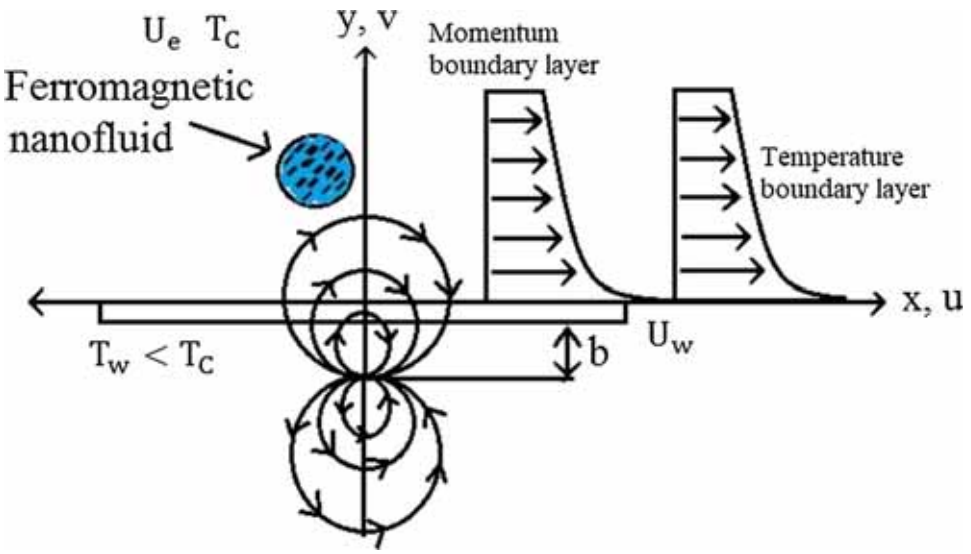

Figure 1. Geometry of the flow framework.

Table 1. Thermophysical properties of water, $NiZnFe_3O_4$, Fe_3O_4, and $MnZnFe_3O_4$.

	ρ (kg/m^3)	C_p(J/kg · K)	k (W/mK)	Pr
Water (H_2O)	998.3	4182	0.60	6.96
$NiZnFe_3O_4$	4800	710	6.3	–
Fe_3O_4	5180	670	9.7	–
$MnZnFe_3O_4$	4700	1050	3.9	–

the temperature at the extending surface $\tilde{T}_w$. The fluid above $\tilde{T}_c$ is not capable of being magnetised. We maintain our study with the hypothesis that the base fluids and nanoparticles are in thermal equilibrium and no slips takes place. In table 1, the thermophysical properties of the nanofluids are discussed. Making use of the stated assumptions, the boundary layer approximation $O(x) = O(1) = O(\tilde{u})$ and $O(y) = O(\delta) = O(\tilde{v})$, the boundary layer equations are

$$\frac{\partial \tilde{v}}{\partial y} + \frac{\partial \tilde{u}}{\partial x} = 0, \tag{1}$$

$$\rho_{nf}\left(\tilde{v}\frac{\partial \tilde{u}}{\partial y} + \tilde{u}\frac{\partial \tilde{u}}{\partial x}\right) = -\frac{\partial p}{\partial x} + M\mu_0\frac{\partial \tilde{H}}{\partial x} + \mu_{nf}\frac{\partial^2 \tilde{u}}{\partial y^2}, \tag{2}$$

$$(\rho C_p)_{nf}\left(\tilde{v}\frac{\partial \tilde{T}}{\partial y} + \tilde{u}\frac{\partial \tilde{T}}{\partial x}\right) + \left(\tilde{v}\frac{\partial \tilde{H}}{\partial y} + \tilde{u}\frac{\partial \tilde{H}}{\partial x}\right)\mu_0\tilde{T}\frac{\partial M}{\partial \tilde{T}} = k_{nf}\frac{\partial^2 \tilde{T}}{\partial y^2}, \tag{3}$$

where $\tilde{u}$ and $\tilde{v}$ represent the components of velocity along x and y directions respectively, μ_{nf} indicates the nanofluid dynamic viscosity, ρ_{nf} exemplifies the nanofluid density, μ_0 is the magnetic permeability, p is pressure, υ_{nf} is the nanofluid kinematic viscosity, k_{nf} is the nanofluid thermal conductivity, $(\rho c_p)_{nf}$ is the specific heat, $\tilde{T}$ is the temperature, $\tilde{H}$ is the magnetic field, and M is the magnetisation.

The relevant boundary conditions for the present problem are thought to be of the form

$$\tilde{u}|_{y=0} = U_w = S_1 x, \quad \tilde{T}|_{y=0} = \tilde{T}_w, \quad \tilde{v}|_{y=0} = 0,$$
$$\tilde{u}|_{y\to\infty} = U_e = S_2 x, \quad \tilde{T}|_{y\to\infty} \to \tilde{T}_\infty = \tilde{T}_c. \tag{4}$$

In eq. (4), U_w and U_e respectively represent the stretching and free stream velocity, $\tilde{T}_w$ is the temperature of the boundaries, and $\tilde{T}_\infty$ is the ambient fluid temperature.

1.2 *Thermophysical properties of* $NiZnFe_3O_4$–H_2O, $MnZnFe_3O_4$–H_2O, *and* Fe_3O_4–H_2O *nanofluids*

The $(\rho c_p)_{nf}$, μ_{nf}, k_{nf}, and the effective dynamic density (ρ_{nf}) of the nanofluid are given as follows:

$$\frac{\mu_{nf}}{\mu_f} = (1-\phi)^{-2.5}, \quad \rho_{nf} = (1-\phi)\rho_f + \phi\rho_s,$$
$$(\rho C_p)_{nf} = (\rho C_p)_f(1-\phi) + (\rho C_p)_s\phi,$$
$$k_{nf} = \frac{(2k_f + k_s) + (k_s - k_f)2\phi}{(2k_f + k_s) - (k_s - k_f)\phi} * k_f. \tag{5}$$

The above general relationship is used to calculate the thermal conductivity, dynamic viscosity, and specific heat of nanofluids, k_f and k_s are the thermal conductivities of the nanoparticle and base fluid respectively, ϕ indicates the solid volume fraction of the nanofluid, ρ_f and ρ_s are respectively the densities of the base fluid and the nanoparticle.

1.3 *Magnetic dipole*

The magnetic field is produced due to magnetic dipole that effects the ferrofluid flow, which is denoted by magnetic scalar potential δ, i.e.

$$\delta = \frac{\gamma_1}{2\pi}\frac{x}{x^2 + (y+d)^2}, \tag{6}$$

where γ_1 denotes the strength of the magnetic field (H) at the source. The H components are of the form

$$\frac{\partial H}{\partial x} = -\frac{\partial \delta}{\partial x} = \frac{\gamma_1}{2\pi}\frac{x^2 - (y+d)^2}{(x^2 + (y+d)^2)^2}, \tag{7}$$

$$\frac{\partial H}{\partial y} = -\frac{\partial \delta}{\partial y} = \frac{\gamma_1}{2\pi}\frac{2x(y+d)}{\left(x^2 + (y+d)^2\right)^2}, \tag{8}$$

since the magnetic body force is (generally) corresponding to the gradient of H, and in this way we have

$$H = \sqrt{\left(\frac{\partial \delta}{\partial y}\right)^2 + \left(\frac{\partial \delta}{\partial x}\right)^2}. \tag{9}$$

Making use of eqs (7) and (8) in eq. (9), we get the progressive equations, after expanding in powers of x and take terms up to order x^2,

$$\frac{\partial H}{\partial x} = -\frac{\gamma_1}{2\pi}\frac{2x}{(y+d)^4}, \tag{10}$$

$$\frac{\partial H}{\partial y} = \frac{\gamma_1}{2\pi}\left(-\frac{2}{(y+d)^3} + \frac{4x^2}{(y+d)^5}\right). \tag{11}$$

The effect of magnetisation (M) with temperature (T) is given by the linear expression below.

$$M = -K_s(T_\infty - T), \tag{12}$$

where K_s denotes the pyromagnetic coefficient. The physical representation of a heated ferrofluid is shown in figure 1. Here the curvy lines show the magnetic field.

2. Solution technique

Here we introduce the accompanying locally similar transformations

$$\psi(x,\ y) = (\nu_\mathrm{f} S_1)^{1/2} x f(\xi), \quad \xi = y\sqrt{\frac{S_1}{\nu_\mathrm{f}}},$$

$$\theta(\xi) = \frac{T_\mathrm{c} - T}{T_\mathrm{c} - T_\mathrm{w}} \tag{13}$$

in which ψ indicates the stream function, $\theta(\xi)$ is the non-dimensional temperature, and the comparable velocity components using similarity transformation u and v are defined as follows:

$$u = \frac{\partial \psi}{\partial y} = S_1 x f'(\xi), \quad v = -\frac{\partial \psi}{\partial x} = -(S_1 \upsilon_\mathrm{f})^{1/2} f(\xi), \tag{14}$$

where prime denotes the differentiation with respect to ξ. By employing similarity transformation (13), eqs (2) and (3) along with presumed boundary conditions (4) give the following form:

$$\frac{1}{(1-\phi)^{2.5}(1-\phi+\phi(\rho_\mathrm{s}/\rho_\mathrm{f}))} f''' - f'^2 + ff'' - \frac{2\beta\theta}{(1-\phi+\phi(\rho_\mathrm{s}/\rho_\mathrm{f}))\,(\xi+\gamma)^4} + R^2 = 0, \tag{15}$$

$$\frac{k_\mathrm{nf}/k_\mathrm{f}}{(1-\phi+\phi[(\rho C_p)_\mathrm{s}/(\rho C_p)_\mathrm{f}])}\theta'' + \mathrm{Pr}\big(f\theta' - 2f'\theta\big) + \frac{2\lambda\beta f(\theta-\varepsilon)}{(\xi+\gamma)^3} - 4\lambda f'^2 = 0, \tag{16}$$

$$f(\xi) = 0, \quad f'(\xi) = 1, \quad \theta(\xi) = 1, \quad \text{at } \xi = 0,$$

$$f'(\xi) \to 0, \quad \theta(\xi) \to 0, \quad \text{when } \xi \to \infty. \tag{17}$$

Here, λ, the viscous dissipation, R, the ratio parameter, ε, the dimensionless Curie temperature, β, the ferrohydrodynamic interaction, and Pr, the Prandtl number are defined as

$$\varepsilon = \frac{T_\infty}{T_\mathrm{c} - T_\mathrm{w}}, \quad \beta = \frac{\gamma}{2\pi}\frac{\mu_0 K(T_\mathrm{c} - T_\mathrm{w})\,\rho}{\mu^2},$$

$$\mathrm{Pr} = \frac{\upsilon}{\alpha}, \quad \lambda = \frac{S_1\mu^2}{\rho k(T_\mathrm{c} - T_\mathrm{w})}, \quad \gamma = \sqrt{\frac{S_1\rho d^2}{\mu}}. \tag{18}$$

2.1 *Skin friction coefficient and local Nusselt number*

The wall shear stress and heat transfer rate are defined as

$$C_\mathrm{f} = \frac{-2\tau_w}{\rho_\mathrm{nf} U_w^2}, \quad \tau_w = \mu_\mathrm{nf}\left.\frac{\partial u}{\partial y}\right|_{y=0},$$

$$\mathrm{Nu} = \frac{x k_\mathrm{nf}}{k_\mathrm{f}(T_\mathrm{c} - T_\mathrm{w})}\left.\frac{\partial T}{\partial y}\right|_{y=0}. \tag{19}$$

We at last accomplished the accompanying dimensionless equations for the skin friction coefficient and heat transfer rate as follows:

$$\frac{1}{2}\mathrm{Re}_x^{1/2} C_\mathrm{f} = \frac{1}{(1-\phi)^{2.5}} f''(0),$$

$$\mathrm{Re}_x^{-1/2}\mathrm{Nu}_x = \frac{k_\mathrm{nf}}{k_\mathrm{f}}\theta'(0), \tag{20}$$

where $\mathrm{Re}_x = xU_w(x)/\upsilon_\mathrm{f}$, the local Reynolds number, is based on the stretching velocity $U_w(x)$, $\mathrm{Re}_x^{1/2} C_\mathrm{f}$ denotes the skin friction, and $\mathrm{Re}_x^{-1/2}\mathrm{Nu}_x$ denotes the Nusselt number.

3. Optimal homotopy analysis method

The solutions of the non-linear ordinary momentum equation (15) and thermal energy equation (16) subjected to the permissible boundary conditions (17) are obtained by using BVPh2-midpoint method (Maple) and OHAM. These procedures are used to get the solutions for boundary value problem (BVP). Compare to other traditional analytical procedure and perturbation technique, the OHAM [35,36] gives better result. Firstly, the OHAM gives us a wonderful opportunity to choose the equation type of linear subproblems. Next, the OHAM works even when there is a probability that there is no large/small physical parameters to decide initial/boundary conditions and equations. Especially, contrary to the perturbation and other investigative techniques, the OHAM allows us an invaluable

way to guaranty the convergence of series solution by exhibiting the convergence governor parameter into the series solution. The linear operators and their initial suppositions with respect to BVP are

$$L_{\mathrm{f}}(f) = \frac{\mathrm{d}^3 f}{\mathrm{d}\xi^3} + \frac{\mathrm{d}^2 f}{\mathrm{d}\xi^2}, \quad L_\theta(\theta) = \frac{\mathrm{d}^2\theta}{\mathrm{d}\xi^2} - \theta, \tag{21}$$

$$f_0(\xi) = 1 - \exp(-\xi), \quad \theta_0(\xi) = \exp(-\xi), \tag{22}$$

where $L_{\mathrm{f}}(f)$ and $L_\theta(\theta)$ denote the linear operators, $f_0(\xi)$ and $\theta_0(\xi)$ are respectively the initial guesses of f and θ.

4. OHAM convergence analysis

The auxiliary parameters h_{f} and h_θ have a main motivation behind controlling the convergence of homotopic solutions. To become convergent solutions, we yield the proposed approximations of these parameters. Consequently, residual errors are seen for momentum, and thermal energy equations by introducing the terminologies given below.

$$\Delta_m^f = \int_0^1 [\mathbf{R}_m^f(\xi, h_{\mathrm{f}})]^2 \mathrm{d}\xi, \tag{23}$$

$$\Delta_m^\theta = \int_0^1 [\mathbf{R}_m^\theta(\xi, h_\theta)]^2 \mathrm{d}\xi. \tag{24}$$

The convergence of the parametric values calculated using OHAM is recorded in table 2 when $\lambda = 0.5$, $\beta = 1.2$, $\mathrm{Pr} = 2.0$, $\gamma = 0.2$, and $\phi = 0.1$ (tables 3, 4).

The graphical illustrations of the 8th- and 10th-order approximation of the error decay are shown in figures 2 and 3. Now Δ_m^t is the total discrete squared residual error

Table 2. The average residual square errors Δ_m^t.

Values→ / Order↓	h_{f}	h_θ	Δ_m^t
4	−0.78901	−0.53131	0.009324
6	−0.94260	−0.72010	5.33150×10^{-8}
8	−0.99832	−0.89031	0.50321×10^{-14}
10	−1.01131	−0.91043	4.28210×10^{-18}
12	−1.05319	−0.99317	2.74090×10^{-23}

Table 3. Demonstrations of individual residual square errors for Δ_m^f and Δ_m^θ.

Values→ / Order↓	$h_{\mathrm{f}} = -1.04319$ Δ_m^f	$h_\theta = -0.98317$ Δ_m^θ
8	7.71010×10^{-22}	2.43890×10^{-16}
10	1.43103×10^{-24}	4.43879×10^{-19}
12	5.19034×10^{-26}	7.55900×10^{-22}
20	8.33298×10^{-28}	0.88231×10^{-24}

Table 4. The comparison of heat transfer rate when $\gamma = \varepsilon = \lambda = \beta = 0$.

Pr	Rashidi *et al* [37]	OHAM results $\mathrm{Re}_x^{-1/2} X^{-1} \mathrm{Nu}_x$	BVPh2-midpoint $\mathrm{Re}_x^{-1/2} X^{-1} \mathrm{Nu}_x$
0.72	0.808631	0.808641	0.808639
1.0	1.000000	1.000000	1.000000
3.0	1.923682	1.923690	1.923672
4.0	–	2.003170	2.003162
5.0	–	2.329810	2.329871
8.0	–	–	2.541990

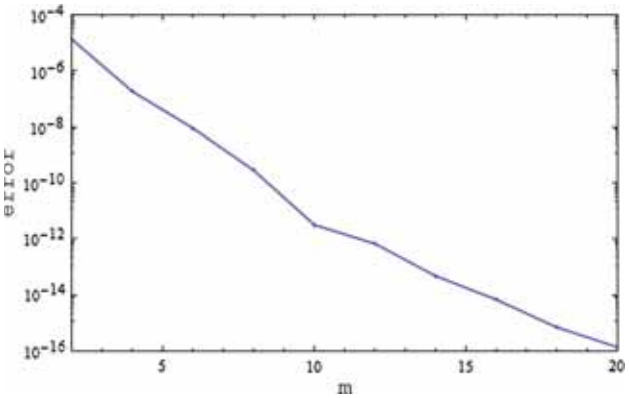

Figure 2. The error decay for the 8th-order approximation.

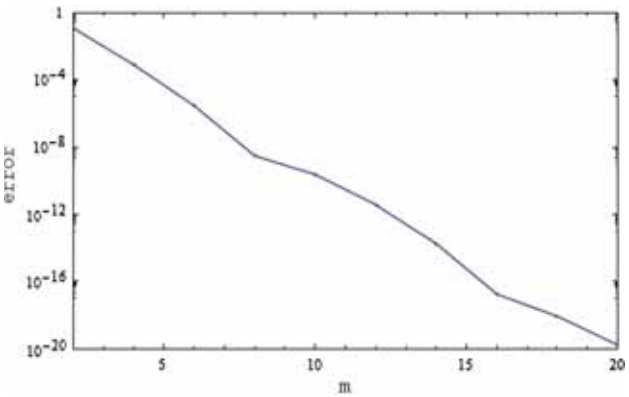

Figure 3. The error decay for the 10th-order approximation.

$$\Delta_m^t = \Delta_m^f + \Delta_m^\theta, \tag{25}$$

where Δ_m^t is used to acquire the optimal convergence governor parameters.

5. Results and discussion

OHAM and BVPh2-midpoint method are used individually to solve BVP analytically and numerically. This section gives us the physical understanding of miscellaneous parameters on the field flow. The effects of

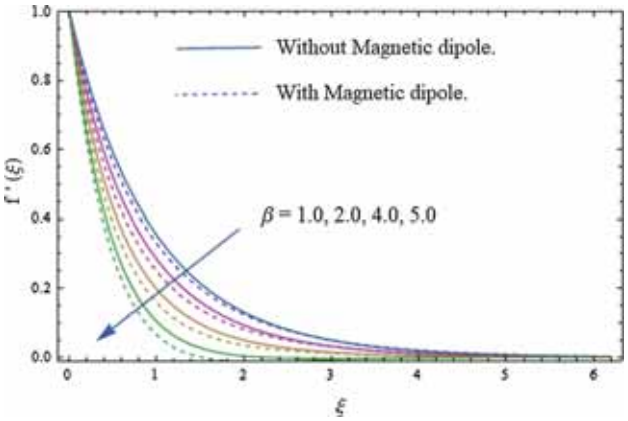

Figure 4. Influence of β on axial velocity.

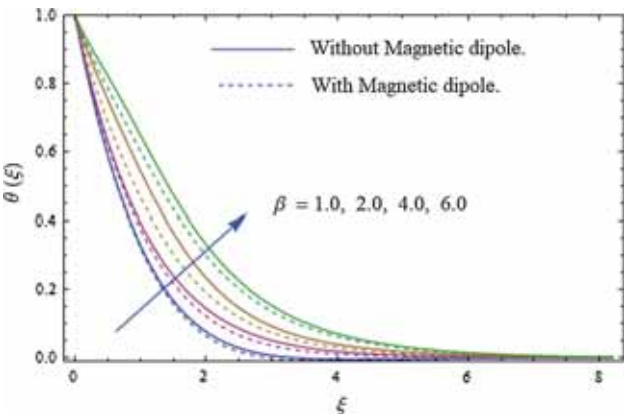

Figure 5. Effect of β on temperature field.

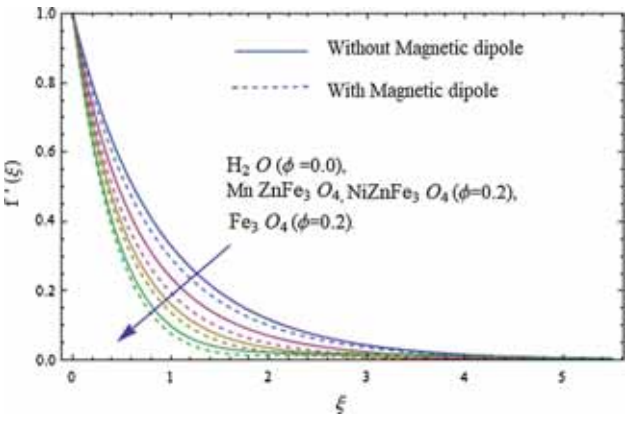

Figure 6. Influence of ϕ on velocity distribution.

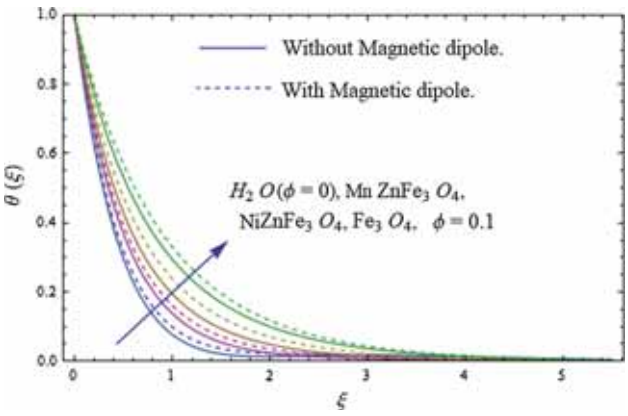

Figure 7. Influence of ϕ on temperature distribution.

submerging dimensionless parameters such as ϕ, β, Pr, and λ are discussed. Also, fixed values are taken for the remaining parameters in a flow problem. The permanent values of these parameters are considered as $\varepsilon = 2.0$, $\lambda = 0.01$, and $\gamma_1 = 1.0$. The precision of the current BVPh2-midpoint and OHAM approach is evaluated by equating $\theta'(0)$ values with those of Rashidi *et al* [37] for water that is classified in table 1. For the special case of the current problem good agreement will occur among the result. The present problem is studied with magnetic dipole and without magnetic dipole. The graphical result is found for the velocity profile, temperature distribution, skin friction coefficient, and heat transfer rate.

Figures 4 and 5 describe the impact of β. To maintain the effect of ferromagnetic impact on the boundary layer flow the occurrence of parameters such as Curie temperature ε, dimensionless distance from origin to centre of magnetic dipole γ and β are necessary. For enlarging β the axial velocity decreases because the fluid viscosity increases for increasing values of β in the presence of Fe_3O_4–H_2O, $NiZnFe_3O_4$–H_2O, and $MnZnFe_3O_4$–H_2O, which is shown in figure 4. The result is found for both the cases with and without magnetic dipole for the velocity profile. It is concluded that the velocity profile diminishes more rapidly in the presence of magnetic dipole than in the absence of magnetic dipole because the magnetic dipole attracts the FNPs and as a result, inside the boundary layer the viscosity of the nanofluid increases which reduces the velocity distribution. The influence of β on temperature distribution is demonstrated in figure 5. The temperature profile enhances for higher values of β for cases with magnetic dipole and without magnetic dipole. It is due to the fact that the interaction of Fe_3O_4–H_2O, $NiZnFe_3O_4$–H_2O, and $MnZnFe_3O_4$–H_2O nanoparticles with magnetic field causes the viscosity to increase which increases frictional heating between fluid layers and as a result velocity diminishes and temperature profile enhances, i.e. reduction in velocity field of FNP enhances the temperature profile. Figures 6 and 7 respectively show the velocity and temperature profiles of $NiZnFe_3O_4$–H_2O, Fe_3O_4–H_2O, and $MnZnFe_3O_4$–H_2O under the influence of ϕ. The axial velocity decreases by increasing ϕ for both cases, i.e., without magnetic dipole and with magnetic dipole. Further, it is noticed

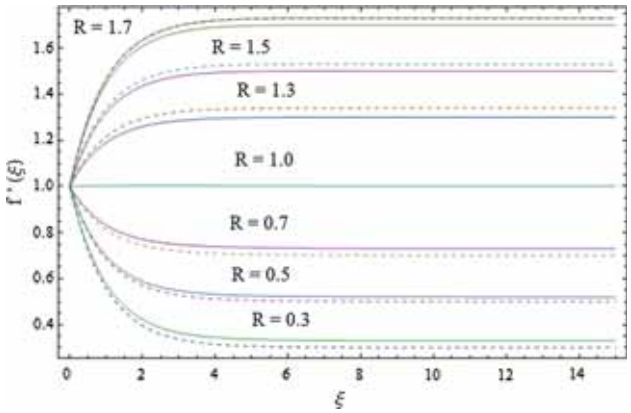

Figure 8. The effect of R on velocity profile.

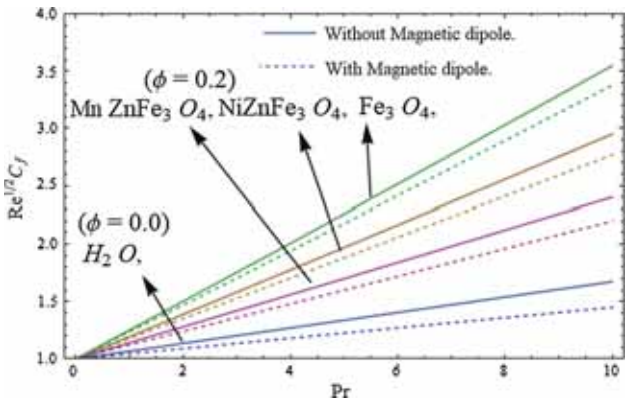

Figure 9. Effect of ϕ on skin friction vs. Pr.

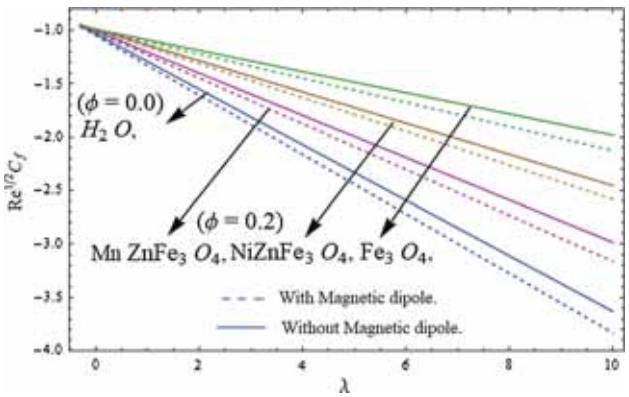

Figure 10. Influence of ϕ on wall shear stress vs. λ.

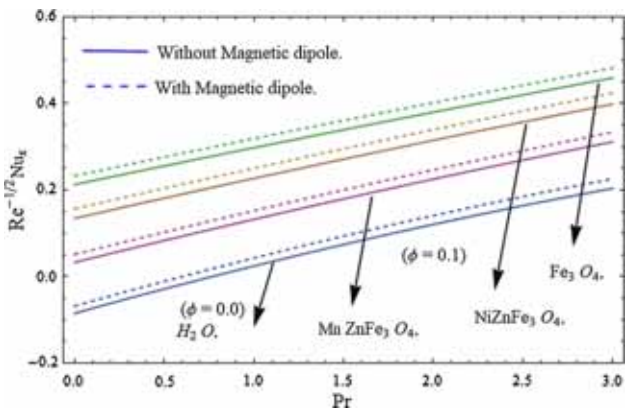

Figure 11. The influence of ϕ on heat transfer rate vs. Pr.

that Fe_3O_4 nanoparticle has lower velocity field than $NiZnFe_3O_4$ and $MnZnFe_3O_4$ because Fe_2O_4 is more magnetic than $NiZnFe_3O_4$ and $MnZnFe_3O_4$. It can be seen from figure 6 that the velocity field rapidly decreases in the presence of magnetic dipole compared to that in the absence of magnetic dipole. Figure 7 demonstrates the temperature field for increasing values of ϕ for both cases, i.e., in the presence and absence of magnetic dipole. The temperature profile increases for cases with magnetic dipole and without magnetic dipole, increasing the value of ϕ. Fe_3O_4 has higher thermal conductivity than $NiZnFe_3O_4$ and $MnZnFe_3O_4$. More thermal conductivity implies that the temperature profile is higher for Fe_3O_4–H_2O than for $NiZnFe_3O_4$–H_2O, and $MnZnFe_3O_4$–H_2O for both cases, i.e. with magnetic dipole and without magnetic dipole. Figure 8 displays the velocity profile of Fe_3O_4–H_2O, $NiZnFe_3O_4$–H_2O, and $MnZnFe_3O_4$–H_2O under the influence of ratio parameter R. R is defined as the ratio of the ambient fluid to surface velocity. The effects of R are accurately characteristic for $R > 1$ and $R < 1$. It is observed that when $R = 1.0$, no boundary layer occurred.

5.1 *Skin friction coefficient and local Nusselt number*

Figures 9–12 show the graphical result for skin friction and Nusselt number. Figures 9 and 10 show the skin friction coefficient of FNPs such as $NiZnFe_3O_4$–H_2O, $MnZnFe_3O_4$–H_2O, and Fe_3O_4–H_2O under the influence of ϕ vs. Pr and λ for both cases, i.e., without and with the influence of magnetic dipole. It is observed that the wall shear stress for H_2O (when $\phi = 0$) is minimum and that for $Fe_3O_4-H_2O$ is maximum because Fe_3O_4 is more magnetised than the other FNPs. So Fe_3O_4 has the highest skin friction profile compared to $NiZnFe_3O_4$, $MnZnFe_3O_4$, and water (H_2O) as is evident in figures 9 and 10. Figures 11 and 12 display the Nusselt number in the presence of magnetic dipole and without magnetic dipole of the ferromagnetic nanofluids such as $NiZnFe_3O_4$–H_2O, $MnZnFe_3O_4$–H_2O, and Fe_3O_4–H_2O for increasing values of ϕ and Pr respectively. Figure 11 shows the Nusselt number profile for increasing values of ϕ of the ferromagnetic nanofluid and Pr for both cases, i.e. without and with magnetic dipole. The heat transfer

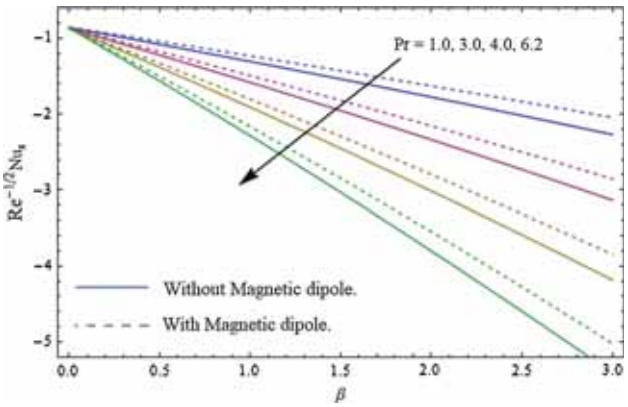

Figure 12. The influence of Pr on heat transfer rate vs. β.

rate is maximum for Fe_3O_4–H_2O, then $NiZnFe_3O_4$–H_2O and $MnZnFe_3O_4$–H_2O with increasing values of Pr. Further, heat transfer rate is higher in the presence of magnetic dipole than in the absence of magnetic dipole, which is depicted in figure 11. Figure 12 demonstrates the effect of Pr vs. β on heat transfer rate in the presence and absence of magnetic dipole. It is observed that Nusselt number diminishes with increasing values of Pr and β. It is also seen that the heat transfer rate decreases fast in the absence of magnetic dipole than in the presence of magnetic dipole (see figure 12). The values allocated to residual parameters are $\beta = 1.0$, $\lambda = 0.3$, and $\Pr = 6.2$.

6. Concluding remarks

The main assumption of this problem is the heat transport phenomenon in a ferromagnetic nanofluid flow in the presence of magnetic dipole. In this article, three different nanoparticles such as Fe_3O_4, $NiZnFe_3O_4$, and $MnZnFe_3O_4$ are discussed with H_2O as the base fluid (or carrier fluid). The BVPh2-midpoint technique and OHAM are utilised respectively to solve this problem numerically and analytically.

The important findings of the current problem are follows:

1. The velocity boundary layer diminishes while the thermal boundary layer enhances by increasing the values of β.
2. In the presence of magnetic dipole, the temperature distribution increases while the axial velocity diminishes with increasing values of ϕ.
3. In the presence of magnetic dipole, Nusselt number decreases drastically.
4. The thermal boundary layer thickness diminishes while the velocity boundary layer enhances for increasing values of Pr.
5. For increasing values of R, the velocity profile increases for both cases, i.e. without and with magnetic dipole.
6. The skin friction coefficients of the ferromagnetic $NiZnFe_3O_4$–H_2O, $MnZnFe_3O_4$–H_2O, and Fe_3O_4–H_2O nanofluids diminish for both cases, i.e., without and with magnetic dipole.

References

[1] X Q Wang and A S Mujumdar, *Int. J. Therm. Sci.* **46**, 1 (2007)
[2] S K Das, S U Choi, W Yu and T Pradeep, *Nanofluids: Science and technology* (John Wiley & Sons, 2007)
[3] S U S Choi and J A Eastman, No. ANL/MSD/CP–84938; CONF-951135–29 (Argonne National Lab., IL, USA, 1995)
[4] S Nadeem and I Shahzadi, *Commun. Theor. Phys.* **64**, 547 (2015)
[5] M Sheikholeslami, R Ellahi and C Fetecau, *Math. Probl. Eng.* **2017**, (2017)
[6] R Tabassum, R Mehmood and S Nadeem, *J. Colloid Interface Sci.* **501**, 304 (2017)
[7] N S Akbar, S Nadeem, T Hayat and A A Hendi, *Heat Mass Transf.* **48**, 451 (2012)
[8] M Ramzan and M Bilal, *J. Mol. Liq.* **215**, 212 (2016)
[9] O D Makinde, *Int. J. Number Method H* **23**, 1291 (2013)
[10] S Khamis, D O Makinde and Y N Gyekye, *Int. J. Number Method H* **25**, 1638 (2015)
[11] S Nadeem, S Ahmad and N Muhammad, *Sensor Actuat. B-Chem.* **263**, 69 (2018)
[12] Y Ma, R Mohebbi, M M Rashidi and Z Yang, *Int. J. Heat Mass Transf.* **137**, 714 (2019)
[13] F Sultan, W A Khan, M Ali, M Shahzad, M Irfan and M Khan, *Pramana – J. Phys.* **92**: 21 (2019)
[14] T Hayat, K Muhammad, M I Khan and A Alsaedi, *Pramana – J. Phys.* **92**: 57 (2019)
[15] A Matori, R Mohebbi, Z Hashemi and Y Ma, *J. Therm. Anal. Calorim.* **136**, 2495 (2019)
[16] M Suleman, M Ramzan, S Ahmad and D Lu, *Phys. Scr.* **94**, 085702 (2019)
[17] J David, *Introduction to magnetism and magnetic materials* (CRC Press, 2015)
[18] R L Bailey, *J. Magn. Magn. Mater.* **39**, 178 (1983)
[19] C D Mee, *Proc. Phys. Soc.* **63**, 922 (1950)
[20] R E Rosensweig, *Annu. Rev. Fluid Mech.* **19**, 437 (1987)
[21] W Voit, D K Kim, W Zapka, M Muhammed and K V Rao, *MRS Online Proceedings Library Archive* 676 (2001)
[22] M Sheikholeslami, R Ellahi and K Vafai, *Alexandria Eng. J.* **57**, 565 (2017)
[23] A Zeeshan and A Majeed, *Alexandria Eng. J.* **55**, 2171 (2016)
[24] C R Vestal and Z J Zhang, *J. Am. Chem. Soc.* **125**, 9828 (2003)

[25] H I Andersson and O A Valnes, *Acta Mech.* **128**, 39 (1998)
[26] N Muhammad and S Nadeem, *Eur. Phys. J. Plus* **132**, 377 (2017)
[27] Y Ma, R Mohebbi, M M Rashidi and Z Yang, *J. Therm. Anal. Calorim.* **136**, 1727 (2019)
[28] D Lu, M Ramzan, S Ahmad, J D Chung and U Farooq, *Phys. Fluids* **29**, 123103 (2017)
[29] Y Ma, R Mohebbi, M M Rashidi, O Manca and Z Yang, *J. Therm. Anal. Calorim.* **135**, 3197 (2019)
[30] D K Singh, D K Pandey, R R Yadav and D Singh, *Pramana – J. Phys.* **78**, 759 (2012)
[31] T Hayat, M Waqas, S A Shehzad and A Alsaedi, *Pramana – J. Phys.* **86**, 3 (2016)
[32] G M Moatimid, M A A Mohamed, M A Hassan and E M M El-Dakdoky, *Pramana – J. Phys.* **92**: 90 (2019)
[33] C Pai, M Shalini and S Radha, *Procedia Engineering* **76**, 79 (2014)
[34] Emran Khoshrouye Ghiasi and Reza Saleh, *Pramana – J. Phys.* **92**: 12 (2019)
[35] A Majeed, A Zeeshan and R Ellahi, *J. Mol. Liq.* **223**, 528 (2016)
[36] S J Liao, *Homotopy analysis method in nonlinear differential equations* (Springer and Higher Education Press, Heidelberg, 2012)
[37] M M Rashidi, N V Ganesh, A K A Hakeem, B Ganga and G Lorenzini, *Int. J. Heat Mass Transf.* **98**, 616 (2016)